A practical water–energy–climate solution for sustainable and resilient coastal cities: smart use of seawater in municipal services

Zi ZHANG
Hong Kong University of Science and Technology https://orcid.org/0000-0003-4673-1717
Yugo SATO
Hong Kong University of Science and Technology https://orcid.org/0000-0002-3896-0176
Ji DAI
Hong Kong University of Science and Technology
Ho-kwong Chui
Hong Kong University of Science and Technology
Glen Daigger
University of Michigan
Mark van Loosdrecht
Delft University of Technology https://orcid.org/0000-0003-0658-4775
Guang-Hao Chen (ceghchen@ust.hk)
HKUST

Analysis

Keywords:

Posted Date: January 10th, 2022

DOI: https://doi.org/10.21203/rs.3.rs-1179774/v1

Title

A practical water–energy–climate solution for sustainable and resilient coastal cities: smart use of seawater in municipal services

Authors

Zi Zhang [1], Yugo Sato [1], Ji Dai [1], Ho-kwong Chui [1], Glen T. Daigger [2], Mark C.M. van Loosdrecht [3], and Guanghao Chen [1, *]

Affiliations

[1] Department of Civil and Environmental Engineering, Chinese National Engineering Research Center for Control & Treatment of Heavy Metal Pollution (Hong Kong Branch) and Water Technology Center, The Hong Kong University of Science and Technology, Hong Kong, China

[2] Civil and Environmental Engineering, University of Michigan, Ann Arbor, Michigan, 48109, USA

[3] Department of Biotechnology, Delft University of Technology, 2628 CD, Delft, The Netherlands

Corresponding author: Guanghao Chen;

Email: ceghchen@ust.hk

Abstract

Municipal services for buildings in developed (sub)tropical coastal cities contributed 18% of greenhouse gases (GHGs) in 2020. One mitigatory solution is the direct use of seawater for district cooling and toilet flushing, which has been applied in Hong Kong on various scales and achieved 30% water and energy savings. However, no systematic evaluation and strategy for this solution are available. Herein, we develop a high-resolution quantitative scheme to elaborate the co-benefits and optimal strategies for expanding this use of seawater. We find that in Hong Kong, Jeddah, and Miami, using local seawater at the city-scale would achieve life-cycle GHG mitigation (42%–56%), energy savings (45%–49%), and freshwater savings (11%–43%). High-resolution analysis reveals that population density and district marginal performance are essential to optimize the efficiency of seawater use. Our scheme confirms the utility of seawater for municipal services and is an effective tool for innovative municipal-service enhancement.

MAIN TEXT

Introduction

The major effects of climate change include intense droughts, water scarcity, flooding, rising sea levels, and seawater intrusions (*1*). The combustion of fossil fuels is responsible for 78% of greenhouse gas (GHG) emissions worldwide, and is thus widely regarded as a leading cause of anthropogenic climate change. Over half of these GHG emissions originate from urbanized coastal regions (<100 km from the sea), where 40% of the global population resides (*2*). These regions account for more than 50% of the world economy and their populations are expected to double by 2050 (*3*, *4*). The high population densities and anthropogenic activities in these regions, and their natural climatic conditions, render them particularly sensitive to climate change (*5*).

One of the most significant repercussions of climate change in coastal regions is increased water stress (*6–8*). Currently, the primary strategies to address these problems are cross-boundary water transportation, seawater desalination, and wastewater reclamation (*9*). However, these strategies are energy-intensive (*10–13*). For instance, cross-boundary water transportation from Guangdong province in mainland China meets 70%–80% of Hong Kong's freshwater needs, and this long-distance transmission consumes over 200 GWh of electricity and releases up to 0.2 $MtCO_2eq$ GHG annually (*14*, *15*). In contrast, seawater desalination is used to generate 50% of Saudi Arabia's freshwater supply, and this consumes up to 14 TWh and emits over 14 $MtCO_2eq$ GHG annually (*16*). Similarly, saltwater intrusion due to the overexploitation of groundwater has led to Florida having the highest annual volume of wastewater reclamation (1.14 million cubic meters (mcm)) of any US state (*17*); however, the energy requirements of a reclaimed water supply (0.5 to 1.0 kWh/m^3) are much higher than those of a typical freshwater supply (0.03 to 0.15 kWh/m^3) (*18*). These examples illustrate that the use of alternative freshwater resources to relieve water stress inevitably increases energy consumption and thus increases GHG emissions.

Another profound consequence of climate change is the alteration in global temperatures. It is predicted that a 1°C increase in global average temperatures by 2050 (compared with today's temperatures) will lead to an average increase in the number of cooling degree days (CDDs) of 25% (*19*). Significant increases of CDDs in (sub)tropical coastal regions lead to tremendous demands for space cooling (*20*, *21*). The International Energy Agency expects that the space-cooling demands of (sub)tropical regions will increase from 14,000 GW to 30,000 GW worldwide by 2050. A water-cooled air-conditioning system typically requires as little as half of the energy required by a conventional air-cooled air-conditioning system. Thus, for a 30,000 GW cooling load, use of the most efficient water-cooled air-conditioning system could result in annual electricity savings of greater than 30,000 TWh compared with a traditional air-cooled system (*22–24*). However, if current trends continue, the water consumption of water-cooled systems will exceed 400 billion m^3 by 2050, which is similar to the national annual water consumption in China (*25–29*). Therefore, although highly efficient water-based space cooling technology saves energy, it intensifies water stress.

Climate change therefore creates a dual problem of water and energy security in hot (sub)tropical coastal regions of the world, such as Hong Kong (HK). Since the 1950s, this problem has been solved in various parts of HK by the direct use of seawater—subsequent to passage through a 5–10 mm coarse screen and electrochlorination treatment—as non-potable water in municipal services (i.e., toilet flushing and district cooling). This achieves the co-benefits of water–energy–GHG emission savings; the freshwater savings from seawater substitution for toilet flushing alone amount to millions of cubic meters annually (*30*, *31*). In particular, the largest seawater-cooled district cooling system has been operating in Kai Tak district since 2013 (*32*). This system is estimated to

have saved 20.3 million kWh electricity from 2013 to 2020, which is equivalent to a 14,210 tCO_2eq GHG reduction (*33*). This successful application of seawater in municipal services in HK suggests that this approach could be a water–energy–climate solution for ensuring the sustainability and resilience of coastal urban areas worldwide (see Fig. 1(a)).

However, the current seawater supply system in HK has not been systematically evaluated and thus comprehensive insights on how such a system can be expanded or applied to other coastal cities are not available. There is therefore a critical need for an explicit understanding of the large-scale water- and energy-savings and environmental impacts of seawater use in municipal services, as its use requires additional operations and infrastructures. In this study, we develop a high-resolution quantitative scheme based on such a joint indicator to elaborate on the co-benefits of seawater usage in municipal services: water–energy savings and GHG mitigation (see Fig. 1b). This universally applicable scheme consists of high-resolution water–energy demand models and a life cycle assessment (LCA) model, which quantify the above-mentioned co-benefits from such seawater usage. It involves a quantitative strategy analysis that is performed by aggregating water, energy, and climate benefits into a joint indicator using a local weighted matrix that reflects the relative importance of water and energy security and GHG mitigation of each city. This analysis is an effective and reliable approach for making trade-off decisions.

We use our high-resolution quantitative scheme to (1) precisely evaluate the water–energy–climate co-benefits of a seawater-based system compared with a traditional freshwater-based system (i.e., business-as-usual [BAU]; see scenarios in the Material and Methods section); (2) determine the localized weightings of water–energy securities and climate change mitigation from 2020 to 2030; (3) assess the high-resolution joint performance and identify the hotspots of a seawater-based system, and thereby determine the optimal expansion strategies; and (4) investigate the factors that are likely to enhance the efficiency of a seawater-based system, namely effective population density, distance to coastlines, and the district marginal performance. Our three study cities are HK and two other typical coastal cities: Jeddah (JD; Saudi Arabia) and Miami (USA; specifically, metropolitan Miami (MM)); all three cities have a hot climate and high living standards, suffer from severe water stress, and have similar demographic characteristics, but have different urban morphologies.

Results

Water–energy–climate co-benefits are achieved from seawater-based municipal services

We employ bottom-up high-resolution water demand models quantify potential district (regional)-level and city-level freshwater savings achieved by the use of seawater in municipal services (i.e., toilet flushing) in HK, JD, MM (Eq. (7)–(8)). These reveal that the annual potential city-level freshwater savings for HK, JD, and MM are 93, 47, and 67 mcm, which accounts for approximately 43%, 23%, and 11% of their respective annual freshwater consumption. At a regional level in each city, the potential freshwater savings in the Yuen Long district (HK), the central east region (JD), and the 81st district (MM) are the highest, being 16, 15, and 11 mcm/year, respectively (Figs. 2a to 2c). We also calculate that the use of seawater in municipal services could result in substantial annual city-level electricity savings, with those in MM being 3.3 and 4.5 times higher than those in HK and JD, respectively (19.3 billion kWh vs. 5.9 and 4.3 billion kWh, respectively) (Figs. 2a to 2c). At a regional level, the North District in HK has the highest electricity saving potential (2.73 billion kWh/year), whereas those in the central east region (JD) and the 81st district (MM) are 1.05 billion and 0.6 billion kWh/year, respectively. Furthermore, we determine that a seawater-cooled district cooling system (DCS) would significantly reduce the energy consumption of buildings and thus reduce their indirect GHG emissions. The energy savings from a seawater-cooled DCS in the

three city case studies are found to be more than 20 times the energy penalty incurred from the large volumes of seawater that must be pumped in such systems (see SI Section VI). In addition, electricity savings are achieved by the seawater-based system through seawater toilet flushing, the treatment of which consumes 90% less electricity than freshwater supply, and by saline wastewater treatment (anaerobic sulfate reduction and sulfide autotrophic denitrification), which uses less energy than conventional wastewater treatment (heterotrophic denitrification and nitrification) (*34*).

To fully assess these in the context of the additional infrastructure and operations required in seawater-based systems, it is necessary to assess the corresponding life cycle environmental impacts. Accordingly, in Fig. 3 we summarize the life-cycle environmental impacts that we calculate for a seawater supply scenario and a BAU scenario for HK, JD, and MM in terms of global warming potential (GWP), ozone formation potential for human health (OFP), fine particulate matter-formation potential (FPFP), marine eutrophication potential (MEP), and marine ecotoxicity potential (METP). It can be seen that the environmental impact intensities for most of the indicators from the seawater supply scenario in HK are less than those for the seawater supply scenario in JD and MM (Fig. 3a). The significantly lower environmental impact intensities for HK reflect the fact that HK is a more compact urban region than JD and MM, with a higher economic density (employment and population density), a higher morphological density (larger floor-to-area ratio and smaller occupant load factor), and more complex mixed land use (*35*). Although the outlook is best for HK, we also find that the seawater supply scenario is clearly superior to BAU scenarios with respect to all impact indicators in MM, and substantially reduces the environmental impacts with respect to non-marine indicators in HK and JD. For example, we calculate that the annual life cycle GHG emissions in the seawater scenario for HK, JD, and MM are 2.7, 7.2, and 13 $MtCO_2eq$, respectively, whereas those for the BAU scenarios are 6.2, 12.4, and 23 $MtCO_2eq$ respectively (Figs. 3b to 3d). An uncertainty analysis of the LCA reveals that the coefficients of variation (CVs) of the results are acceptable. We also calculate the paybacks for a seawater-based municipal services system in the three cities, and reveals that these paybacks are shorter than the life expectancy of the systems (SI Section VII).

Contextualized dynamic weighting factors are defined for optimal planning

To systematically plan the use of seawater to supply municipal services, we devise a weighting matrix to integrate the multidimensional and geographically varying water–energy savings and GHG mitigations. Figure 4 illustrates the weightings for three indicators—water security, energy security, and GHG mitigation—for use in decision-making on seawater usage in municipal services in HK, JD, and MM from 2020 to 2030. In HK and MM, the models show that GHG reduction goals are the most important factor in decision-making, and their importance increases between 2021 and 2030 by 15.5% and 32.4% for HK and MM, respectively (HK: 0.58 in 2021 to 0.67 in 2030; MM: 0.74 in 2021 to 0.98 in 2030). In JD, however, the models show that GHG reduction goals are not the most important factor in this decision-making, and their importance decreases yearly by 30% in JD (i.e., 0.14 to 0.098). In JD, the models indicate that engineered water is the most important factor in this decision-making, which reflects the fact that Saudi Arabia is one of the most water-scarce nations on the planet and thus faces substantial challenges in ensuring water security; nevertheless, its importance increases yearly by only 4.7% (0.86 to 0.90). Conversely, the models show that the importance of engineered water increases the most in HK (by 27.4%; from 0.062 to 0.079), which implies that future water security in HK will increasingly rely on engineered water.

High-resolution data reveal the optimal strategy for use of seawater in municipal services

As shown in the high-resolution results (Fig. S5), the use of seawater in municipal services does not synchronously generate large savings in water usage or energy usage, or reductions in GHG emissions, where these are measured by three independent indexes: a water performance index, an energy performance index, and an environmental performance index, respectively. In particular, high values for these performance indexes are scattered widely in HK and JD, whereas they are more aggregated in MM. Rows 1 to 3 in Fig. 5 shows the analyzed results of modeling the use of seawater-based municipal services in these cities. In HK, the Yuen Long district has the highest water-performance index (0.192), the North district has the highest energy-performance index (0.465), and the Island district has the highest environmental performance index (0.131). In JD, the central east region has the highest water and environmental performance indexes (0.52 and 0.44, respectively), whereas the central region has the highest energy performance index (0.45). Finally, in MM, the 81st district has the highest water performance index (0.158), and the 96th district has the highest energy and environmental performance indexes (0.119 and 0.123, respectively).

The joint performance index is formed by using the weighting matrix (Fig. 4) to integrate the three independent performance indexes. The grid-level joint performance of the seawater supply in the three cities in 2020 shows that HK has fewer areas with high joint-performance values than JD and MM, and that HK has a more even distribution of higher-value areas than JD and MM (see Fig. S5). The district-level results (the last row in Fig. 5) show that in HK the North and Island districts have the highest joint-performance values (0.195 and 0.112, respectively); in JD, the central-eastern, central, and southwestern regions have the highest joint-performance values (0.512, 0.449, and 0.197, respectively); and in MM, the 96th, 102nd, and 81st districts have the highest joint-performance values (0.122, 0.113, and 0.113, respectively). A comparison of the independent performance index and joint performance index results illustrates that these give different orders of priority for areal deployment of a seawater supply system for municipal services. For instance, in HK, the top three districts in terms of independent water performance are Yuen Long > Sha Tin > Tuen Mun; the top three districts in terms of independent energy performance are North > Island > Yau Tsim Mong; and the top three districts in terms of independent environmental performance are Island > Tsuen Wan > Yuen Long. In contrast, the top three districts in terms of joint performance are North > Island > Yuen Long.

Essential factors for seawater-based municipal services, generalized from our high-resolution analysis

Upper panel Figures 6a to 6c depict the relationships between the grid-level joint performance of seawater-based municipal services and the effective population densities of the three cities. It can be seen that in all three cities there is a consistent increase in joint performance as the effective population density increases. In addition, the variability of the joint performance is higher when the effective population density is less than 5,000 people/km^2 than when it is greater than 5,000 people/km^2, which implies that water–energy–GHG savings are not always obtained under the former conditions. Figures 6d to 6f show that the maximum distance of HK, JD, and MM from their respective coastlines to building sites is less than 50 km; however, there is no significant correlation between the joint performance and this distance. Similarly, Figs. 6g to 6i illustrate the relationship between the population served by municipal services utilizing seawater and the district-level cumulative joint performance of such services in the cities. As can be seen, the marginal performance varies significantly between districts in HK and MM but is more consistent between districts in JD. HK is the most compact of the three cities, and the marginal performances of seawater-based municipal services in the Island and Tsuen Wan districts are clearly high; in comparison, the marginal performances of seawater-based municipal services in the North, Yuen Long, and Sha Tin districts are lower, despite the high joint performance of such services in these

districts. The marginal performances of seawater-based municipal services in MM vary somewhat between districts.

Co-benefits of seawater-based municipal services vary between cities

The above assessment indicates that the co-benefits of seawater-based municipal services vary between cities. To determine which of our three study cities could achieve higher contextualized co-benefits in terms of water–energy–GHG emission savings, we calculate the population-normalized city-level joint significance from 2021 to 2030 using Eqs. 17 and 18. This city-level indicator integrates the benefits of seawater-based municipal services for reducing a given area's local water–energy stress and facilitating achievement of its GHG mitigation goals. Consequently, the variation in the benefits of seawater-based municipal services can be compared between locations. Figure 6 lower panel demonstrates that MM benefits the most from seawater-based municipal services, despite the decrease in benefits from 2023 (8.15×10^{-7}) to 2027 (7.20×10^{-7}). JD derives the next-highest benefits from seawater-based municipal services (5.28×10^{-8} to 3.50×10^{-8}), and HK the least ($\sim 3.25 \times 10^{-8}$); however, the benefits in HK are more consistent and increase from 2020 to 2030. Overall, these results show that seawater-based municipal services have a higher potential to ensure water–energy security and enable the achievement of GHG emission reductions in MM than in HK or JD.

Discussion

More than half of the 17 United Nations Sustainable Development Goals (UNSDGs) of the UN 2030 Agenda for Sustainable Development address social and environmental issues (*36*). Typically, efforts to fulfill a water–energy–climate goal result in synergies between the three aspects of the goal or a trade-off between one aspect and the other two (*37*). However, incorporating dynamic weighting factors for a given region can facilitate a suitably tailored decision-making process that accounts for the region's requirements for water and energy security and climate change mitigation. It follows that although the abatement of GHG emissions is a global goal, it is a priority to fulfill the basic needs of a given region suffering from extreme water or energy shortages (*38*, *39*). The localized dynamic weighting method in this study thus reflects the nexus of requirements for water and energy security, and climate change mitigation, in a specific region. This aids in the formulation of developmental strategies that consider the actual demands of a region, thereby guaranteeing water and energy security for its adequate socio-economic development and also contributing to the achievement of global GHG reduction goals. Such an understanding of the various long-term dynamic weightings of different regions of the world is critical for achieving the UNSDGs.

To combat anthropogenic climate change, HK aims to decrease its GHG emissions by 30% by 2030, which is equivalent to a decrease of 14 $MtCO_2eq$ per year (*40*). In this context, the city-level introduction of seawater-based municipal services in HK, including toilet flushing and district cooling, will realize life cycle annual GHG reductions of up to 3.5 $MtCO_2eq$ per year, i.e., 25% of the 2030 target, thus strongly contributing to a reduction in GHG emissions generated in the supply of municipal services to buildings. Although energy security is less of a problem in JD than in HK and MM, climate change affects all parts of the world, including Saudi Arabia. Specifically, climate change-driven increased temperatures and decreased rainfall will exacerbate water stress in Saudi Arabia, decrease groundwater recharge, and increase surface runoff (*41*). It is therefore significant that our modeling reveals that city-level seawater supply to municipal services in JD would achieve 34.5% of its population-averaged annual GHG reduction goal (15 $MtCO_2eq$) (*42*), which is significant in a region dependent on fossil fuels. However, compared with HK and JD, there is a

greater absolute reduction in GHG emissions in MM due to the implementation of city-level seawater-based municipal services, and this reduction contributes to 18% of the population-based 2030 GHG reduction target for MM (56 $MtCO_2eq$) (*43*).

High-income regions typically solely use high-quality freshwater for municipal services and neglect opportunities to use diverse water sources for various domestic purposes (*44*). Seawater is the most reliable and resilient water source in coastal regions and it is also safer for human health to use seawater, rather than reclaimed water (treated effluent), to replace freshwater in municipal services (*45*). This is because the salinity of seawater serves as a clear warning of cross-contamination of freshwater with seawater due to pipe misconnection. In contrast, the contamination of freshwater with reclaimed water due to pipe misconnection is less easily detectable and thus poses significant risks to human health, and is the major barrier to the large-scale application of reclaimed water for toilet flushing.

Despite the above-described benefits of seawater-based municipal services as a practical means to achieve water–energy–climate co-benefits in coastal cities, especially given the maturity of the associated technical aspects, multiple challenges are associated with their use, and there are limitations to our assessment. The greatest challenges of using seawater are the need to prevent seawater mains failure and the unpredictable source contamination of seawater; this creates the need for well-managed regular maintenance and constant monitoring of seawater at source. In the 50 years that seawater has been used for toilet flushing in HK, there were fewer recorded annual seawater mains failures and leaks than in the parallel freshwater system (2,022 and 2,106 mains bursts and leaks in the freshwater supply, and 34,079 and 6,392 in the seawater supply) (*46*). Furthermore, a study of 200 years of groundwater chemistry data revealed that there have been no significant impacts resulting from seawater leakage to groundwater from pipes supplying seawater to municipal services (*47*).

Materials and Methods

Determination of the localized weightings of water and energy security, and GHG mitigation

The local priorities for water and energy security and GHG mitigation are assessed in terms of the equivalent carbon emissions from engineered water (i.e., cross-boundary water transportation or seawater desalination), imported energy (fossil fuels or electricity), and GHG reduction goals. We calculate the equivalent carbon emissions (EC) by multiplying the carbon intensity of the GDP (CI) and the costs of imported energy and engineered water. Historical (2010–2019) EC data for imported energy and engineered freshwater are input into an ARIMA model to forecast the equivalent GHG emissions to 2030 (see Eq. (1)). The finalized parameters (p, d, q) for the ARIMA model are summarized in Table S9. The GHG mitigation goals are annualized into the equivalent quantities of carbon reduction ($EC_{\text{mitigation}}$) from 2020 to 2030. The dynamic weighting matrix is determined by the EC emissions from each component divided by the total equivalent carbon emissions of the three factors (see Eq. (2)). Data for historical and projected engineered water, imported energy, and GHG mitigation goals are summarized in SI Section V.

$$(1 - \sum_{i=1}^{p} p_i L^i)(1 - L)^d X_t = (1 + \sum_{i=1}^{q} q_i L^i)\epsilon_t \quad (1)$$

$$W_{decision_{i,t}} = \left[\frac{EC_{energy_{i,t}}}{EC_{i,t}} \quad \frac{EC_{water_{i,t}}}{EC_{i,t}} \quad \frac{EC_{mitigation_{i,t}}}{EC_{i,t}} \right]_{10\times 3} \quad (2)$$

$$EC_{i,t} = EC_{energy_{i,t}} + EC_{water_{i,t}} + EC_{mitigation_{i,t}} = C_{energy}{}_{i,t} CI_{i,t} + C_{water}{}_{i,t} CI_{i,t} + EC_{mitigation,i,t} \quad (3)$$

where L is the lag operator; d is the difference number; ϵ is the noise; p is the autoregressive coefficient; X are the equivalent carbon emissions; q_i is the moving average coefficient; EC is the equivalent GHG emissions ($tCO_2eq/year$); C is the monetary costs (USD/year); and CI is the carbon intensity of GDP (tCO_2eq/USD).

Overall high-resolution quantitative assessment scheme

Gross floor area (GFA) and effective population density (EPD) are the two critical parameters for the water and energy demand models. The GIS data for residential and commercial land use in HK, JD, and MM (see Fig. S2–S4) are obtained from GIS databases, and are disassembled into 1 km^2 tiles for HK and JD and into 5 km^2 tiles for MM, based on these cities' geographic scales. We convert land-use data into a GFA using the floor-to-area ratio (FAR), and the effective population densities are calculated using the occupant load factor (OLF) and the calculated GFA. The water and energy demand models are used to quantify the water and energy demands in each grid. We conduct an LCA by inputting the population density-allocated infrastructure inventory and operation inventory of the seawater supply to calculate the environmental impacts at the grid level. The values of the performance indexes of water savings, energy savings, and GHG mitigation are determined for each tile. In addition, these three performance indexes are joined into a single index by using the local weighting matrix. District- or regional-level joint performance is determined by assembling the grid-level results. The assessment framework and assessment boundary are depicted in Fig. S1, and the computations are performed in ArcMap 10.6 (Esri, Redlands, California USA).

Grid-level GFA and EPD determinations

The original NextGIS land-use data of the three cities in the study, including residential and commercial types, are obtained and then disassembled into each predefined grid. The areas of each type of land use (LUA) are calculated in ArcMap 10.6. Briefly, the grid-level GFA of each type of building (residential and commercial) is calculated in terms of its FAR (see Eq. (4)), which is the initial step for GFA determination. Then, the population in each grid is determined using the OLF (see Eq. (5)) (*48–50*), and the convergence of the total population with the actual population is calculated (see Eq. 6). The calculated population is converged to the actual population with adjustment of the FAR, and then the final GFA in each grid is determined (convergence = 1). The initial FARs and OLFs of each type of land use and building are based on the local building design codes, and the adjustment of the FAR parameter is within these design codes (*51*, *52*).

$$GFA = FAR_t \times LUA \ (4)$$

$$Pop_{cal}{}_{j,t} = max\{\frac{GFA_{non-domestic,j,t}}{OLF_t}, \frac{GFA_{domestic,j,t}}{OLF_t}\} \ (5)$$

$$Covergence = \frac{\sum_{j=1} Pop_{cal}{}_{j,t}}{Pop_{act}} \ (6)$$

where j is the grid ID; t is the iterative parameter; Pop_{cal} is the calculated population and Pop_{act} is the actual population; GFA is the gross floor area (m^2); OLF is the occupant load factor (m^2/person); FAR is the floor-to-area ratio; and LUA is the area of land use (m^2).

Water and energy demand models

The demand for seawater (WD_{SW}) includes seawater for a DCS (WD_{DCS}) and toilet flushing (WD_{TF}) (see Eq. (7)). The volume of seawater required for cooling is determined by the amount of heat that must be removed from an indoor environment and the design cooling range of the cooling water

(typically 5℃). The amount of heat is determined by the CDDs and the GFA in a specific location. The freshwater savings (see Eq. (8)) result from the replacement of freshwater with seawater in toilet flushing.

$$WD_{SW_{i,j}} = WD_{DCS_{i,j}} + WD_{TF_{i,j}} = \sum_{k=1}^{2} \frac{C_{air}\rho_{atm} n_k GFA_{j,k} h_k \Delta T_{air_i}}{C_w \Delta T_{cw} \rho_w} + Pop_{i,j} N_{TF}^* V_{TF}^* \quad (7)$$

$$FWS_{i,j} = WD_{TF_{i,j}} \quad (8)$$

where i is the city; j is the grid ID; k is the land use or building type, including residential and non-residential types; n is the number of air exchanges per day; h is the height of a floor (m); N^*_{TF} is the daily number of toilet flushes per person; and V^*_{TF} is the average flushing volume (m^3/flushing).

In this study, the energy demands of a seawater supply for toilet flushing and district cooling (ED_{SW}) and the conventional freshwater supply for freshwater toilet flushing and decentralized cooling (ED_{BAU}) are constructed. The total energy demand is the sum of all water processing and treatment components (see Eqs. (9) and (10)). Energy savings (*ES*) is the difference between the energy demands of the seawater supply scenario and the BAU scenario.

$$ED_{SW_{i,j}} = WD_{SW_{i,j}} \sum_{a=1}^{4} EUI_a + WD_{TF_{i,j}} \sum_{c=1}^{2} EUI_c + \sum_{k=1}^{2} \frac{(C_{air}\rho_{atm} n_k V_{j,k} \Delta T_{air_i})}{EER_{wc}} \quad (9)$$

$$ED_{BAU_{i,j}} = WD_{TF_{i,j}} \sum_{b=1}^{3} EUI_b + WD_{TF_{i,j}} \sum_{c=1}^{2} EUI_c + \sum_{k=1}^{2} \frac{(C_{air}\rho_{atm} n_k V_{j,k} \Delta T_{air_i})}{EER_{Ac}} \quad (10)$$

$$ES_{i,j} = ED_{BAU_{i,j}} - ED_{SW_{i,j}} \quad (11)$$

where EUI is energy use intensity (kWh/m^3); EER_{wc} and EER_{AC} are the energy efficiency ratio of a water-cooled DCS and a conventional air-cooled cooling system; a represents the processes related to seawater (pumping from source, treatment, mains distribution, and lifting to storage tank); b represents the processes related to freshwater (treatment, distribution, and lifting to storage tank); c represents the wastewater treatment processes (a sulfate reduction, autotrophic denitrification, and nitrification integrated process for the seawater supply scenario and an anaerobic/oxic wastewater treatment for the BAU scenario, and sludge handling).

LCA model

The assessment boundary is defined in Fig. 8(b) and the functional unit is defined as the annual seawater supply and space cooling services provided to the population. In this study, the operational and infrastructural life cycle inventories (LCIs) are considered in the assessment. The quantities of newly built infrastructures on a city level are determined by two approaches: (1) if there is a similar entry to the required new infrastructure in the Ecoinvent 3.0 database, the quantity of the new infrastructure is calculated based on this existing entry; (2) if there is no existing entry, manufacturers' fact sheets are utilized to determine how much equipment and materials are needed for the given flow rates or cooling loads. The function GenerateNearTable in ArcMap 10.6 is utilized to determine the length of the additional water-distribution pipe, and the results represent the distances from the coastline to the infrastructure sites. This approach may overestimate material usage; however, this overestimation means that the LCI is conservative and thus has no negative effects on the performance assessment. Next, an infrastructure allocation model (modified from an empirical road development model) is applied to quantify the infrastructure attributed to each grid (see Eq. (12)) (*53*). The newly built infrastructures in each tile are then normalized by their corresponding life expectancy. Subsequently, the corresponding life cycle impact-assessment (LCIA) metrics, including all of the entries in the LCI, are generated by the ReCiPe Midpoint (H) method on the SimaPro platform. The LCIA of the seawater supply system at the grid level is

calculated by multiplying the LCI matrix and metrics matrix. For the BAU scenario, only the operational phase need be considered in the LCI. The detailed assumptions and LCI are given in SI Section III and IV.

$$AF_{i,j} = \frac{\left(0.684EPD_j^{-0.274}ICPC_i^{0.657}\right)Pop_{cal,j}}{\sum_1^j\left(0.684EPD_j^{-0.274}ICPC_i^{0.657}\right)Pop_{cal,j}} \quad (12)$$

where $AF_{i,j}$ is the infrastructure allocation factor; EPD is the effective population density (people/km^2); and ICPC is the income per capita (USD/capita).

Grid-level independent and joint performance index

The performance index (*PI*) is the proportion of water and energy savings and GHG mitigation in each tile (see Eqs. (13) to (15)). A *PI* value is a dimensionless number ranging from 0 to 1, where larger values correspond to greater benefits. The joint performance index integrating water, energy, and environmental performance is calculated by multiplying the independent *PI* values and the dynamic weighting matrix (see Eq. (16)).

$$PI_{water_{i,j}} = \frac{WD_{TF_{i,j}}}{\sum_1^j(WD_{TF_{i,j}})} \quad (13)$$

$$PI_{energy_{i,j}} = \frac{ED_{BAU_{i,j}} - ED_{SW_{i,j}}}{\sum_1^j(ED_{BAU_{i,j}} - ED_{SW_{i,j}})} \quad (14)$$

$$PI_{environmental_{i,j}} = \frac{GWP_{BAU_{i,j}} - GWP_{SW_{i,j}}}{\sum_1^j GWP_{BAU_{i,j}} - GWP_{SW_{i,j}}} \quad (15)$$

$$PI_{i,j} = \left[PI_{energy_{i,j}} \quad PI_{water_{i,j}} \quad PI_{environmental_{i,j}}\right]_{j\times 3}$$

$$PI_{joint_{i,j,t}} = PI_{i,j}W^T_{decision_{i,t}} \quad (16)$$

Population-averaged joint significance

A city-level joint significance index is calculated to represent the variation in the importance of seawater-based municipal services supply between locations. Thus, the quantities of saved water and energy and reduced GHG emissions are divided by the corresponding projected demands for engineered water, imported energy, and GHG mitigation in a given city. The city-level joint indexes are then integrated by the localized weighting matrix.

$$PI_{city_{i,t}} = \left[\frac{FWS_i}{Water_{eng_{i,t}}} \quad \frac{ES_i}{Energy_{impt_{i,t}}} \quad \frac{GHG_{BAU-SW}}{GHG_{mtg_{i,t}}}\right]_{10\times 3} \quad (17)$$

$$PI_{pop_{joint_{i,t}}} = PI_{city_{i,t}}W^T_{decision_{i,t}}Pop^{-1}_{city,i} \quad (18)$$

where FWS_i, ES_i, and $GHG_{BAU\text{-}SW}$ are the city-level freshwater saving, energy saving, and GHG reduction achieved by using a seawater-based system; $Water_{eng_{i,t}}$, $Energy_{impt_{i,t}}$, and $GHG_{mtg_{i,t}}$ are the projected demands for engineered water, imported energy, and GHG reduction; and $Pop^{-1}_{city,i}$ is the reciprocal of the city-level population.

References

1. T. Oakes, *Climate change 2007 Impacts, Adaptation, and Vulnerability* (Cambridge University Press, United Kingdom, 2009).
2. Q. He, M. D. Bertness, J. F. Bruno, B. Li, G. Chen, T. C. Coverdale, A. H. Altieri, J. Bai, T. Sun, S. C. Pennings, J. Liu, P. R. Ehrlich, B. Cui, Economic development and coastal ecosystem change in China. *Sci. Rep.* **4**, 1–9 (2014).
3. The Ocean Conference, "The ocean conference fact sheet" (The Ocean Conference, United Nations, New York, 2017).
4. L. Creel, Ripple effects: Population and coastal regions. *Popul. Ref. Bur.* **8**, 1–6 (2003).
5. E. Fleming, J. Payne, W. V Sweet, M. Craghan, J. Haines, J. Finzi-Hart, H. Stiller, A. Sutton-Grier, Coastal Effects. *Impacts, Risks, Adapt. United States Fourth Natl. Clim. Assessment, Vol. II*. **II**, 322–352 (2018).
6. C. and S. Department, 2019-2021 Hong Kong Gross Domestic Product, implicit price deflator of GDP, and per capita GDP (2021).
7. H. E. T. R. Saud, Distribution of gross domestic product contributions in Saudi Arabia in 2014, by province (Saudi Arabia HVAC-R Market Outlook 2021, page 27, December 2016)].
8. Bureau of Economic Analysis, GDP by states 4th quarter 2020 and annual 2020 (available at https://www.bea.gov/news/2021/gross-domestic-product-state-4th-quarter-2020-and-annual-2020-preliminary).
9. World Bank, Water scarce cities: Thriving in a finite world. *Int. Bank Reconstr. Dev.*, **65**, 7–14 (2018).
10. M. Molinos-Senante, D. González, Evaluation of the economics of desalination by integrating greenhouse gas emission costs: An empirical application for Chile. *Renew. Energy*. **133**, 1327–1337 (2019).
11. T. Michou, Water and greenhouse gases: The desalination challenge. *Am. Bar Assoc. J.* **19**, 14 (2016).
12. A. Tal, Addressing desalination's carbon footprint: The Israeli experience. *Water (Switzerland)*. **10**, 1–20 (2018), doi:10.3390/w10020197.
13. Doingjiang Water. *HK Water Supplies Dep.* (available at https://www.wsd.gov.hk/en/core-businesses/water-resources/dongjiang-water/index.html).
14. WSD, Hong Kong: the facts-water supplies. *HK WSD* (available at https://www.wsd.gov.hk/en/publications-and-statistics/pr-publications/the-facts/index.html).
15. Electricity Consumption. *Census Stat. Dep. HK* (available at https://www.censtatd.gov.hk/en/web_table.html?id=127).
16. S. M. H. Bin Marshad, "Economic evaluation of seawater desalination: A case study analysis of cost of water production from seawater desalination in Saudi Arabia," thesis, Heriot-Watt University (2014). https://www.ros.hw.ac.uk/handle/10399/2996
17. Sea Level Rise Task, Force, Report on Flooding and Salt Water Intrusion, 187 (2016).
18. National Research Council, *Water Reuse: Expanding the Nation's Water Supply Through Reuse of Municipal Wastewater Understanding the Risks* (2011).
19. International Energy Agency (IEA), "The Future of Cooling Opportunities for energy-efficient air conditioning," International Energy Agency Website: www.iea.org, 2018 (2018) (available at www.iea.org).
20. EMSD, Hong Kong Energy End-use Data (HKEEUD) 2019 (2019).
21. X. Liao, J. W. Hall, N. Eyre, Water use in China's thermoelectric power sector. *Glob. Environ. Chang.* **41**, 142–152 (2016).
22. C. H. Yip, W. Y. Ho, Enhancing Building Energy Efficiency-A Concerted Effort of the Trade and the Government. *4th Gt. Pearl River Delta Conf. Build. Oper. Maint.*, 103 (2013).

23. Energy Efficiency Impact Report, Efficiency Opportunities (2018) [https://energyefficiencyimpact.org/].
24. Office of Energy Efficiency and Renewable Energy, Commercial buildings integration program (2020).
25. F. W. H. Yik, J. Burnett, I. Prescott, Study on the energy performance of three schemes for widening application of water-cooled air-conditioning systems in Hong Kong. *Energy Build.* **33**, 167–182 (2001).
26. Y. Zhou, Comparison of Chinese green building standard with Western green building standards. *KTH Eng. Manag.*, **30**, 2–30 (2014).
27. APERC, Towards zero-emission efficient and resilient buildings GLOBAL STATUS REPORT 2016, 1–32 (2001).
28. IEA, The Future of Cooling: Opportunities for energy-efficient air conditioning. *Futur. Cool. Oppor. Energy-efficient Air Cond.* 92 (2018).
29. S. Hall, H. Pix, Laboratories for the 21st Century : Water Efficiency Guide for Laboratories, United States Environmental Protection Agency
30. R. W. K. Leung, D. C. H. Li, W. K. Yu, H. K. Chui, T. O. Lee, M. C. M. Van Loosdrecht, G. H. Chen, Integration of seawater and grey water reuse to maximize alternative water resource for coastal areas: The case of the Hong Kong International Airport, *Water Sci. Technol.* **65**, 410–417 (2012).
31. X. Liu, J. Dai, T. L. Ng, G. Chen, Evaluation of potential environmental benefits from seawater toilet flushing. *Water Res.* **162**, 505–515 (2019).
32. N. Ribeiro, Legislative Council Panel on Environmental Affairs Collection of Charges for District Cooling System at the Kai Tak Development. **14** (2014).
33. HKSAR, District Cooling System (2021), (available at https://www.veolia.com/middleeast/sites/g/files/dvc171/f/assets/documents/2016/07/District_Cooling_System_ME_EN.pdf).
34. D. Wu, G. A. Ekama, H. K. Chui, B. Wang, Y. X. Cui, T. W. Hao, M. C. M. van Loosdrecht, G. H. Chen, Large-scale demonstration of the sulfate reduction autotrophic denitrification nitrification integrated (SANI®) process in saline sewage treatment. *Water Res.* **100**, 496–507 (2016).
35. G. M. Ahlfeldt, E. Pietrostefani, The compact city in empirical research: A quantitative literature review. *Spat. Econ. Res. Centre, London*, 73 (2017).
36. UNSDGS The 17 Goals (available at https://sdgs.un.org/goals).
37. C. Dyngeland, J. A. Oldekop, K. L. Evans, Assessing multidimensional sustainability: Lessons from Brazil's social protection programs. *Proc. Natl. Acad. Sci. U. S. A.* **117**, 20511–20519 (2020).
38. OECD, "OECD ENVIRONMENT DIRECTORATE AND INTERNATIONAL ENERGY AGENCY" (2004).
39. T. Gore, Extreme Carbon Inequality: Why the Paris climate deal must put the poorest, lowest emitting and most vulnerable people first. *Oxfam Media Brief.*, 1–14 (2015).
40. "CLIMATE ACTION PLAN 2030+" (Hong Kong, 2017) (available at https://www.enb.gov.hk/sites/default/files/pdf/ClimateActionPlanEng.pdf).
41. E. M. Darfaoui, A. Al Assiri, Response to Climate Change in the Kingdom of Saudi Arabia, 1–17 (2009).
42. Climate Transparency, "Brown to Green: The G20 Transition to a Low-carbon Economy," Saudi Arabia Facts (2011).
43. Fact Sheet: President Biden Sets 2030 Greenhouse Gas Pollution Reduction Target (2021) [https://www.whitehouse.gov/briefing-room/statements-releases/2021/04/22/fact-sheet-president-biden-sets-2030-greenhouse-gas-pollution-reduction-target-aimed-at-creating-good-paying-union-jobs-and-securing-u-s-leadership-on-clean-energy-technologies/].

44. United States Environmental Protection Agency (EPA), Potential Contamination Due to Cross-Connections and Backflow and the Associated Health Risks, 44 (2001).
45. "CHAPTER 8 Water Supplies Department Managing and reducing water main bursts and leaks" (2010) [https://www.aud.gov.hk/pdf_e/e55ch08.pdf].
46. C. M. Leung, J. J. Jiao, Change of groundwater chemistry from 1896 to present in the Mid-Levels area, Hong Kong. *Environ. Geol.* **49**, 946–959 (2006).
47. Florida Department of Education, Florida Building Code Handbook, State Requirements for New Educational Facilities Construction (2010).
48. C. Hopkin, M. Spearpoint, D. Hopkin, Y. Wang, Residential occupant density distributions derived from English Housing Survey data. *Fire Saf. J.* **104**, 147–158 (2019).
49. L. T. Wong, Occupant Load Factor in Local Residential Old High-Rise Buildings. *Int. J. Eng. Performance-Based Fire Codes*. **6**, 197–201 (2004).
50. American Society of Planning Officials, "Floor Area Ratio" (1958), Chicago, Illinois.
51. Planning Department, Chapter 2 Residential Densities. *Hong Kong Plan. Stand. Guidel.*, 1–34 (2018).
52. J. L. Simon, D. R. Glover, *12. The Effect of Population Density on Infrastructure: The Case of Road Building* (2014).
53. Buildings Department, Code of Practice for Fire Safety in Buildings. *Building Department HK* (2011) [https://www.bd.gov.hk/doc/tc/resources/codes-and-references/code-and-design-manuals/fs2011/fs2011_full.pdf].

Acknowledgments

Funding:
The Hong Kong Research Grants Council (no. T21-604/19-R)
Hong Kong Innovation and Technology Commission (no. ITC-CNERC14EG03).

Author contributions:
Conceptualization: ZZ, JD, GHC
Methodology: ZZ, JD
Investigation: ZZ
Visualization: ZZ, GTD, MCMvL
Supervision: GHC
Writing—original draft: ZZ
Writing—review & editing: ZZ, YS, JD, HKC, GTD, MCMvL, GHC

Competing interests: The authors declare no competing interest.

Data and materials availability: All data are available in the main text or in supplementary materials.

628 **Figures**

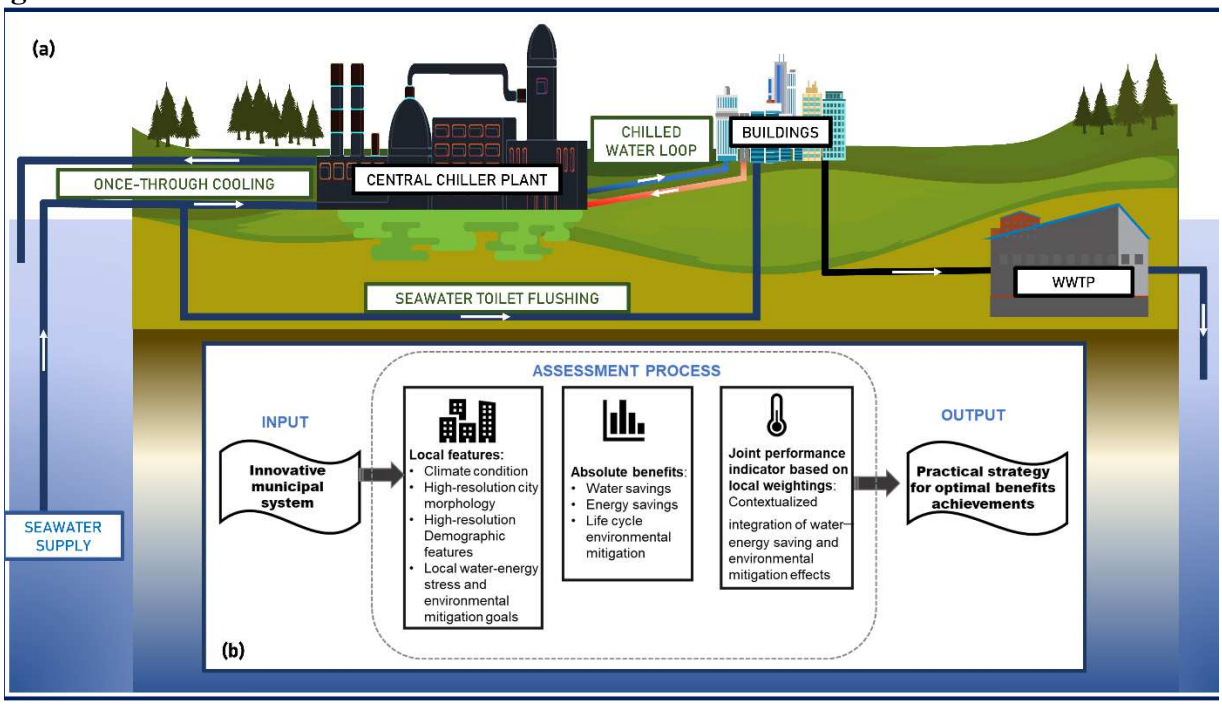

629
630 **Figure 1. Illustration of the seawater-based municipal services system and the high-resolution**
631 **quantitative assessment scheme (a)** Graphical demonstration of seawater-based municipal service
632 system for toilet flushing and a DCS; **(b)** quantitative high-resolution assessment scheme for such
633 a system. In this study, the input is the seawater supply and the output is the practical strategy that
634 optimizes the water–energy–GHG emissions savings in a city. WWTP: wastewater treatment plant.
635

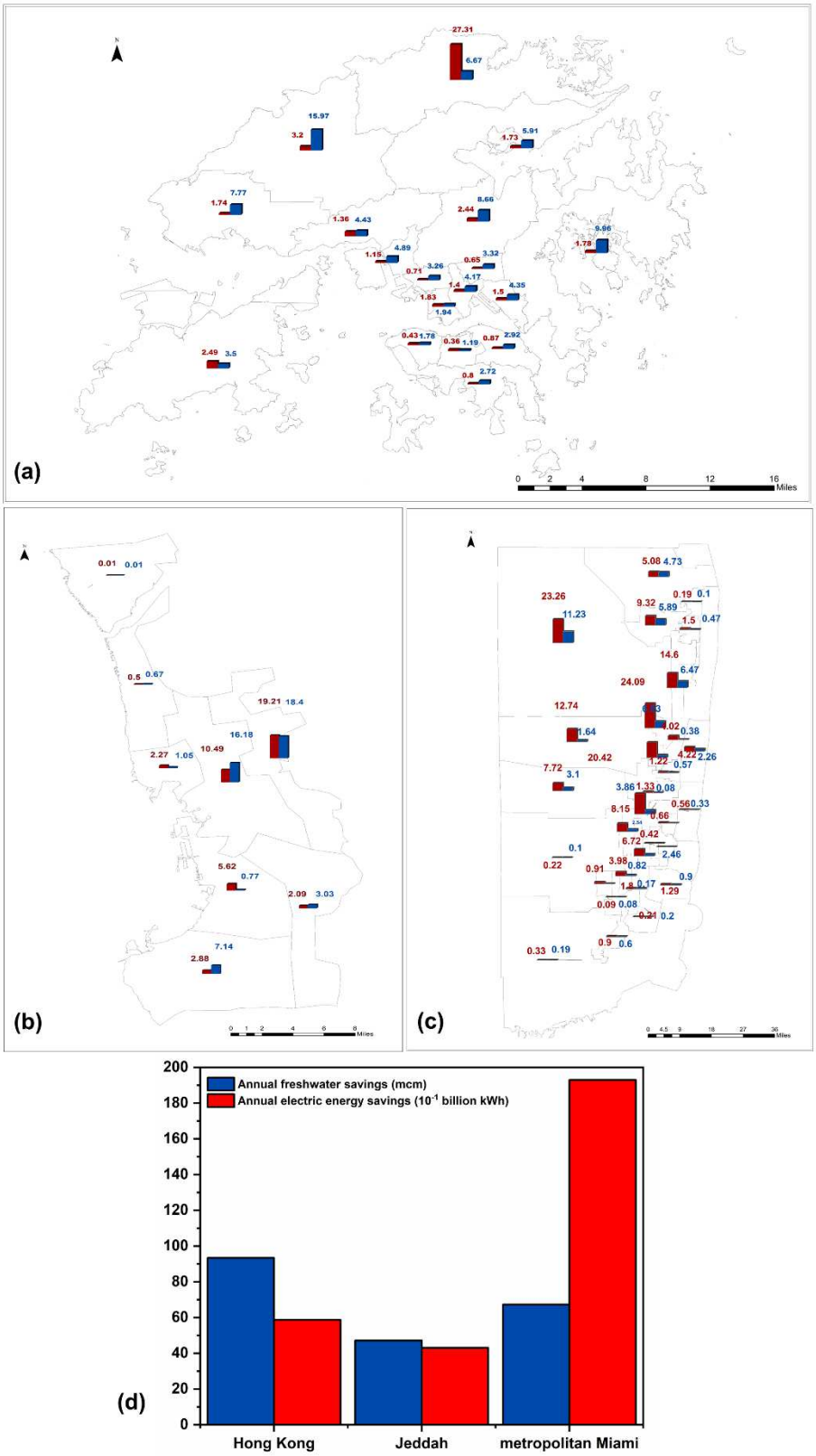

Figure 2. District and city-level water-energy synergies achieved from a seawater-based municipal services system. (a) to **(c)** District-level annual freshwater savings and electricity savings from the city-wide seawater-based municipal service system in HK, JD, and MM; **(d)** aggregated annual benefits from this system.

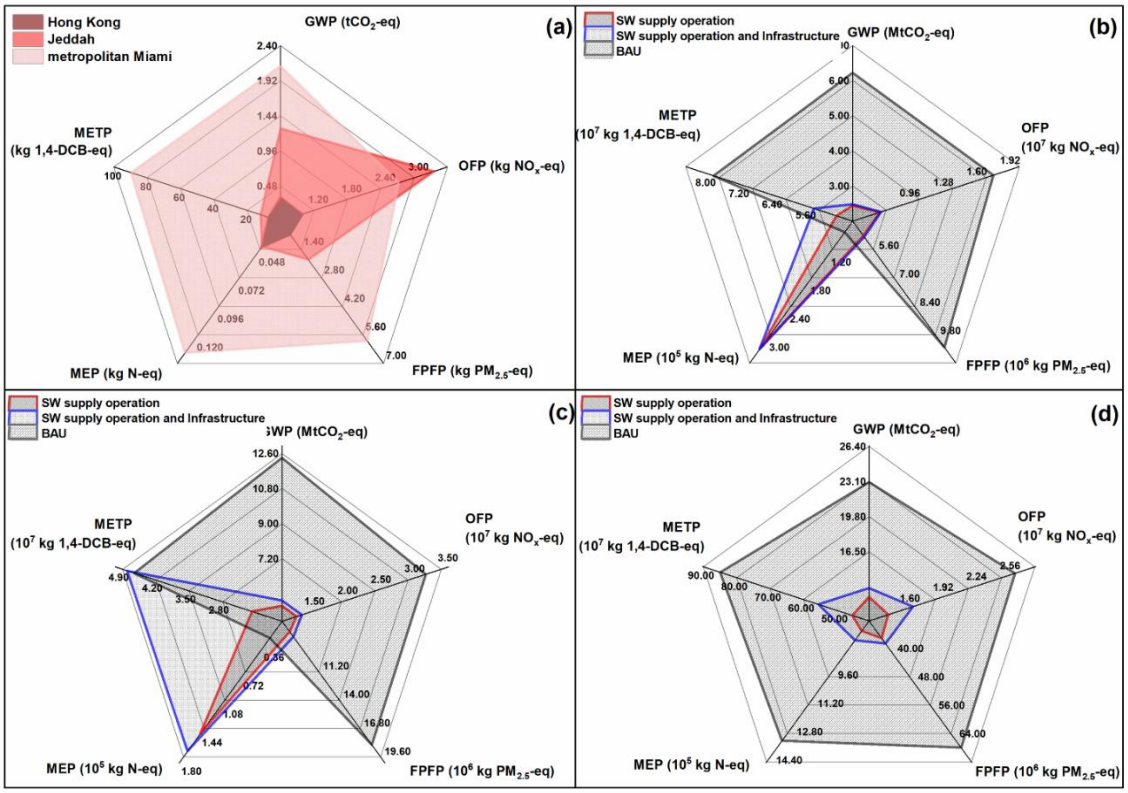

Figure 3. Life cycle environmental impacts of a seawater (SW)-based municipal service system (a) Intensities of life cycle environmental impact from the SW system in three cases (unit: impact/person/year); **(b)**–**(d)** annualized life cycle impacts (LCIA) of city-wide SW system scenarios without and with infrastructures, and the business-as-usual (BAU; baseline) scenario in Hong Kong, Jeddah (Saudi Arabia), and metropolitan Miami (Florida, USA). GWP: global warming potential; OFP: ozone formation potential; FPFP: fine particulate formation potential; MEP: marine eutrophication potential; METP: marine ecotoxicity potential.

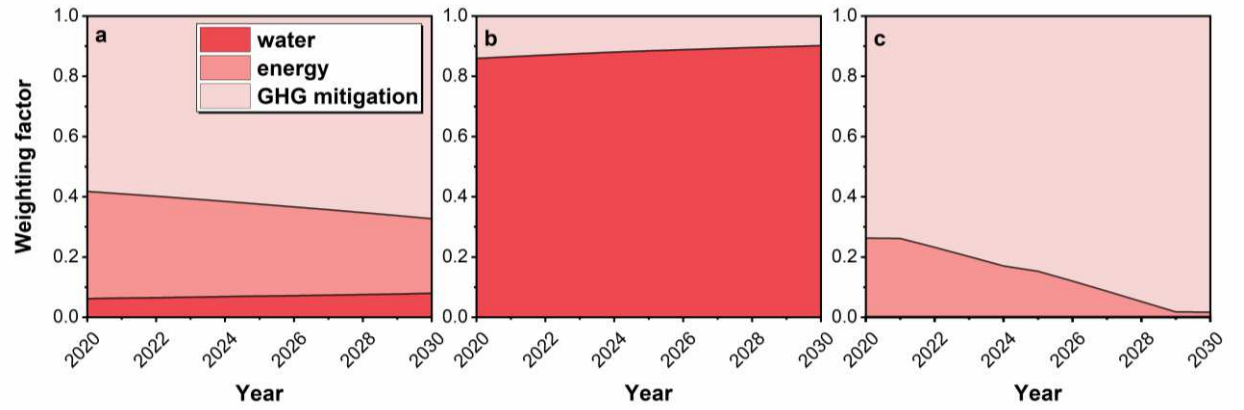

Figure 4. Dynamic weighting factors (relative importance of water and energy security, and GHG mitigation) of the three cities studied (a: Hong Kong, b: Jeddah, c: metropolitan Miami) from 2020 to 2030. These factors are calculated by normalizing the equivalent carbon emissions of the engineered water, imported energy, and GHG mitigation goals for each city. The autoregressive integrated moving average (ARIMA) models predict future equivalent carbon emissions from historical data on engineered water and imported energy for an area; as JD and MM are not economic entities, historical data for Saudi Arabia and the United States are used to generate their respective ARIMA models.

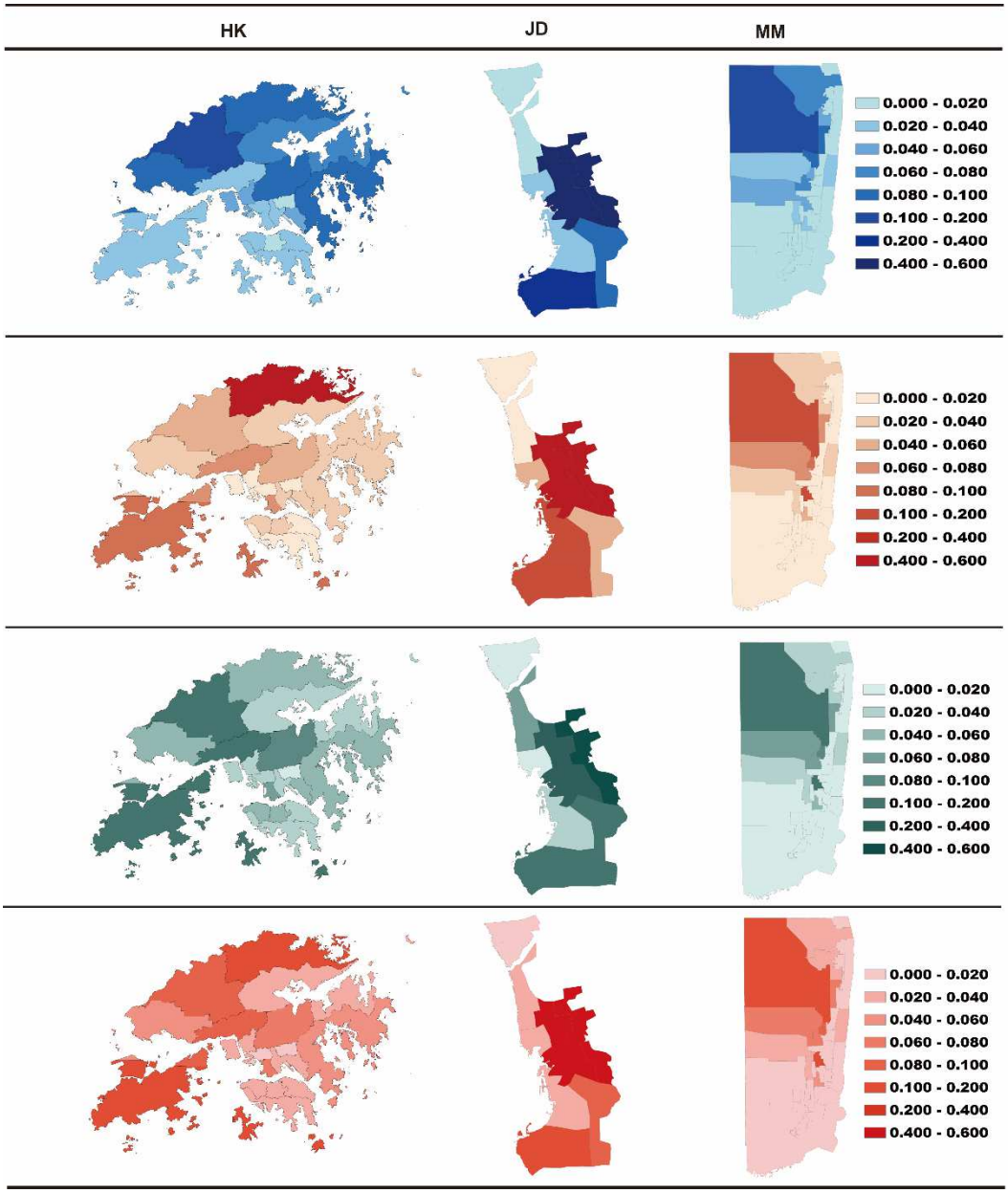

Figure 5. District-level independent performance in water–energy–GHG emission savings and joint performances in the three study locations (Hong Kong (HK), Jeddah (JD), and metropolitan Miami (MM)). **Row-1**: District-level independent water performance index; **row-2**: district-level independent energy performance index; **row-3** district-level independent environmental performance index; **row-4**: district-level joint performance index. The water, energy, and environmental performances of each district are the shared benefits of this district, and the joint performance index is the integration of three independent performance indexes by the local weighting matrix.

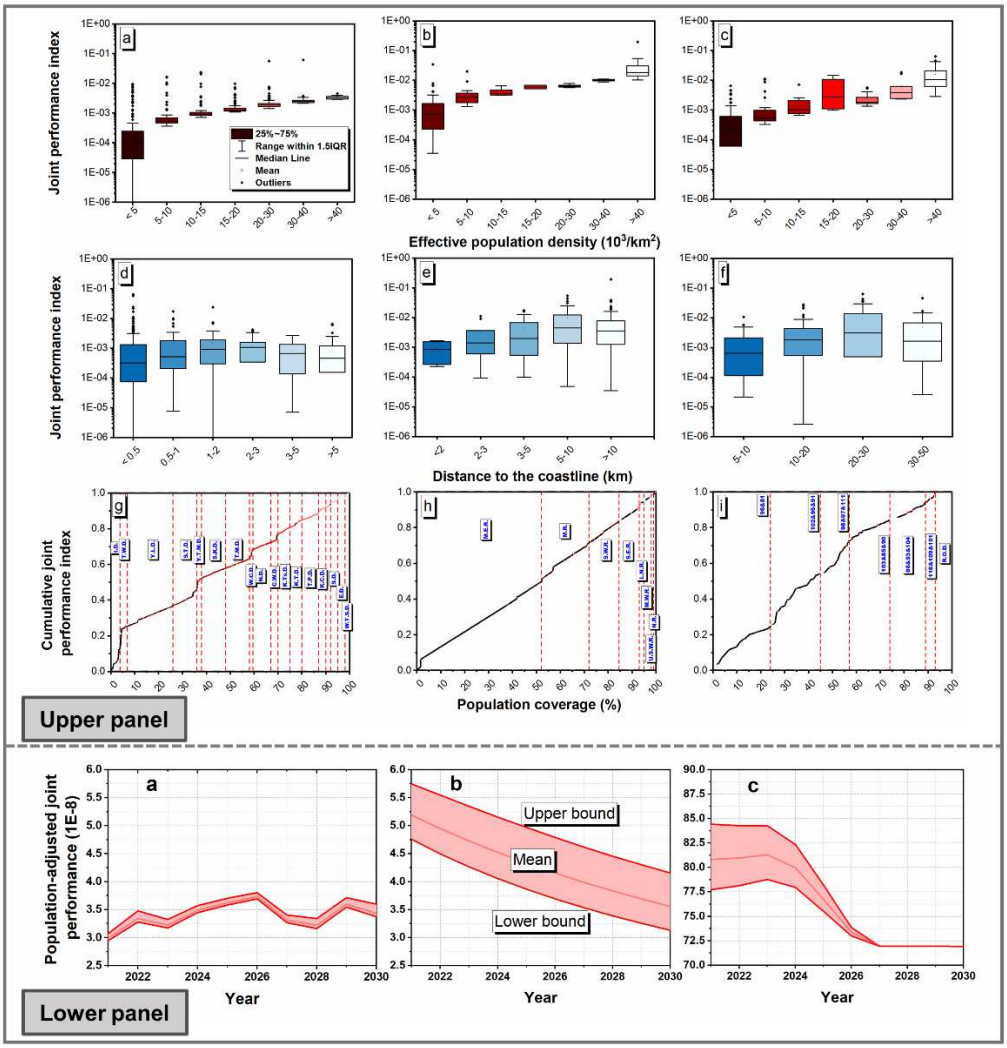

Figure 6. Upper panel: Parameters related to the overall performance of a seawater-based municipal services system. (a)–(c): Grid-level joint performance index vs. effective population density in Hong Kong, Jeddah, and metropolitan Miami; **(d)–(f)**: Grid-level joint performance index vs. distance from the application site to coastline; **(g)–(i)**: Cumulative grid-level joint performance index vs. population coverage of a seawater-based municipal services system. The red dashed lines indicate different districts; the boxes with blue text show the abbreviations of the district names, and the list of full names of districts are summarized in Figs. S1 to S3; **Lower panel**: **City-level population-normalized joint performance of the seawater-based municipal services system from 2020 to 2030 in three cities: (a)**, **(b)**, and **(c)** are Hong Kong, Jeddah, and metropolitan Miami, respectively.

Supplementary Files

This is a list of supplementary files associated with this preprint. Click to download.

- Equivalentcarbons.xlsx
- SIonly.pdf
- LandusewithgridID.xlsx
- Pipedata.xlsx
- Gridleveldataandresults.xlsx